








RESEARCH ARTICLE | MARCH 30 2021

# Long-range spin-wave propagation in transversely magnetized nano-scaled conduits

Special Collection: [Mesoscopic Magnetic Systems: From Fundamental Properties to Devices](#)

Björn Heinz ; Qi Wang ; Michael Schneider; Elisabeth Weiß; Akira Lentfert; Bert Lägél ; Thomas Brächer; Carsten Dubs ; Oleksandr V. Dobrovolskiy ; Philipp Pirro ; Andrii V. Chumak 



*Appl. Phys. Lett.* 118, 132406 (2021)  
<https://doi.org/10.1063/5.0045570>



Boost Your Optics and Photonics Measurements

Lock-in Amplifier

Zurich Instruments

Find out more

Boxcar Averager

# Long-range spin-wave propagation in transversely magnetized nano-scaled conduits

Cite as: Appl. Phys. Lett. **118**, 132406 (2021); doi: [10.1063/5.0045570](https://doi.org/10.1063/5.0045570)

Submitted: 27 January 2021 · Accepted: 12 March 2021 ·

Published Online: 30 March 2021



View Online



Export Citation



CrossMark

Björn Heinz,<sup>1,a)</sup> Qi Wang,<sup>2</sup> Michael Schneider,<sup>1</sup> Elisabeth Weiß,<sup>2</sup> Akira Lentfert,<sup>1</sup> Bert Lägel,<sup>3</sup> Thomas Brächer,<sup>1</sup> Carsten Dubs,<sup>4</sup> Oleksandr V. Dobrovolskiy,<sup>2</sup> Philipp Pirro,<sup>1</sup> and Andrii V. Chumak<sup>2</sup>

## AFFILIATIONS

<sup>1</sup>Fachbereich Physik and Landesforschungszentrum OPTIMAS, Technische Universität Kaiserslautern, D-67663 Kaiserslautern, Germany

<sup>2</sup>Faculty of Physics, University of Vienna, A-1090 Wien, Austria

<sup>3</sup>Nano Structuring Center, Technische Universität Kaiserslautern, D-67663 Kaiserslautern, Germany

<sup>4</sup>INNOVENT e.V. Technologieentwicklung, D-07745 Jena, Germany

**Note:** This paper is part of the APL Special Collection on Mesoscopic Magnetic Systems: From Fundamental Properties to Devices.

<sup>a)</sup>Author to whom correspondence should be addressed: [bheinz@rhrk.uni-kl.de](mailto:bheinz@rhrk.uni-kl.de)

## ABSTRACT

Magnonics attracts increasing attention in the view of low-energy computation technologies based on spin waves. Recently, spin-wave propagation in longitudinally magnetized nano-scaled spin-wave conduits was demonstrated, proving the fundamental feasibility of magnonics at the sub-100 nm scale. Transversely magnetized nano-conduits, which are of great interest in this regard as they offer a large group velocity and a potentially chirality-based protected transport of energy, have not yet been investigated due to their complex internal magnetic field distribution. Here, we present a study of propagating spin waves in a transversely magnetized nanoscopic yttrium iron garnet conduit of 50 nm width. Space and time-resolved microfocused Brillouin-light-scattering spectroscopy is employed to measure the spin-wave group velocity and decay length. A long-range spin-wave propagation is observed with a decay length of up to  $(8.0 \pm 1.5) \mu\text{m}$  and a large spin-wave lifetime of up to  $(44.7 \pm 9.1) \text{ns}$ . The results are supported with micromagnetic simulations, revealing a broad single-mode frequency range and the absence of a mode localized to the edges. Furthermore, a frequency nonreciprocity for counter-propagating spin waves is observed in the simulations and the experiment, caused by the trapezoidal cross section of the structure. The revealed long-distance spin-wave propagation on the nano-scale is particularly interesting for an application in spin-wave devices, allowing for long-distance transport of information in magnonic circuits and low-energy device architectures.

© 2021 Author(s). All article content, except where otherwise noted, is licensed under a Creative Commons Attribution (CC BY) license (<http://creativecommons.org/licenses/by/4.0/>). <https://doi.org/10.1063/5.0045570>

Magnonics, the research field of spin-wave based data transport and information processing, aims to complement CMOS-based computation technology by replacing the charge-based binary logic with a wave-based logic.<sup>1–4</sup> Utilizing spin waves as information carriers provides a variety of advantages such as a high energy efficiency due to the absence of Ohmic losses<sup>5–7</sup> and additional degrees of freedom since frequency and phase of a spin wave are readily accessible.<sup>8</sup> Moreover, spin-wave systems inherit a multitude of nonlinear mechanisms<sup>9–11</sup> while being scalable to the nano-scale,<sup>12,13</sup> allowing for a unique device architecture<sup>14,15</sup> and simultaneously reducing the device feature size to sizes comparable to or even smaller than their CMOS-based equivalent.<sup>16</sup> A large number of spin-wave based devices and logic elements have been realized in recent years, such as transistors,

majority gates,<sup>17,18</sup> or directional coupler,<sup>11,16</sup> with many more theoretical concepts proposed.<sup>19–21</sup> While being well investigated on the macro- and microscale, the study of nano-sized magnonic elements has just scratched the surface due to the limited spin-wave propagation distance on this scale and the difficulties accompanying the fabrication of nano-sized magnetic elements. Only recent progress pushed the go-to material of magnonics, yttrium iron garnet (YIG), to the nano-scale<sup>12</sup> revealing a reasonably large exponential decay length of  $1.8 \mu\text{m}$  in longitudinally magnetized YIG nano-conduits.<sup>13</sup> Although a further perfection of material growth or the usage of different materials with improved characteristics might allow for an increase in the spin-wave propagation length, it is already apparent that the dominating loss channels in such systems are not intrinsic processes,<sup>22</sup> but extrinsic

scattering processes mediated by lattice defects, surface roughness, or magnetic inhomogeneities.<sup>13</sup> Thus, approaches to avoid and eliminate these scattering processes are of great interest. Among them, the transport of information using topologically protected (e.g., based on the Dzyaloshinskii–Moriya interaction<sup>23–25</sup>) or backscattering immune (caused by the intrinsic spin-wave mode chirality) spin-wave states is investigated. As it has been shown recently, magnetostatic surface waves (MSSWs<sup>22</sup>) feature such a backscattering immunity to surface defects due to the presence of energy gaps in the volume mode spectrum, rendering them insensitive to significant structural defects.<sup>26</sup> In addition, in commonly used nanometer thick micrometer-sized structures, MSSWs are known to provide a much larger group velocity in comparison to other spin-wave modes<sup>22,27</sup> (see the [supplementary material](#) for a detailed comparison), which renders these waves an interesting subject of investigation regarding a long-distance data transport in magnonic circuits. However, MSSWs require a transverse magnetization state, leading to a strongly nonuniform internal magnetic field distribution in laterally confined nano-structures, which causes the formation of localized edge-mode states and separated center-mode states.<sup>28–30</sup> For nano-scaled conduits, this field nonuniformity is even more pronounced and, in addition, a strong quantization is present, resulting in a complex interplay. Therefore, the mode structure in transversely magnetized nano-scaled systems is still an open question.

Here, we report on the investigation of propagating spin waves in a transversely magnetized nano-sized YIG conduit of 50 nm width. We show that spin waves can propagate in such a waveguide in spite of the strong nonuniformity of the internal magnetic field, observing a large spin-wave decay length up to 8  $\mu\text{m}$ . In addition, a nonreciprocity for counter-propagating spin waves is observed, which opens up the path for different device architectures. The experimental findings are supported with micromagnetic simulations, revealing a broad single-mode frequency range and the absence of a mode localized to the edges.

In this study, a thin lanthanum-doped (111) YIG film of 44 nm thickness is used, which is grown by liquid phase epitaxy<sup>7,31</sup> on top of a 500  $\mu\text{m}$  thick (111) gadolinium gallium garnet substrate. A characterization of the plain film by means of vector network analyzer ferromagnetic resonance spectroscopy<sup>32</sup> and microfocused Brillouin-light-scattering (BLS) spectroscopy<sup>33</sup> revealed the following material parameters: saturation magnetization  $M_s = (140.7 \pm 2.8)$  kA  $\text{m}^{-1}$ , Gilbert damping parameter  $\alpha = (1.75 \pm 0.08) \times 10^{-4}$ , inhomogeneous linewidth broadening  $\mu_0 \Delta H_0 = (0.18 \pm 0.01)$  mT, and exchange constant  $A_{\text{ex}} = (4.22 \pm 0.21)$  pJ  $\text{m}^{-1}$ . These parameters are within the typical range for high-quality thin YIG films.<sup>7,31</sup> Nanoscopic waveguides were fabricated using a hard mask ion beam milling procedure,<sup>15</sup> resulting in conduits with a trapezoidal cross section. The bottom of the structure is 85 nm wide, while the top width is as narrow as 50 nm, which was determined by scanning electron microscopy (see [Fig. 1](#)). Afterward, a gold coplanar waveguide (CPW) antenna was added on top of the waveguide with a center-to-center distance of ground and signal line of 1.2  $\mu\text{m}$ , a linewidth of 500 nm, and a thickness of 160 nm. In the experiment, a large bias magnetic field of  $\mu_0 H_{\text{ext}} = 270$  mT is applied in-plane along the short axis of the structure to ensure a transversely magnetized state. Radio frequency (RF) continuous-wave (cw) currents or pulses with a length of 50 ns and a repetition time of 350 ns are generated and fed into the CPW antenna

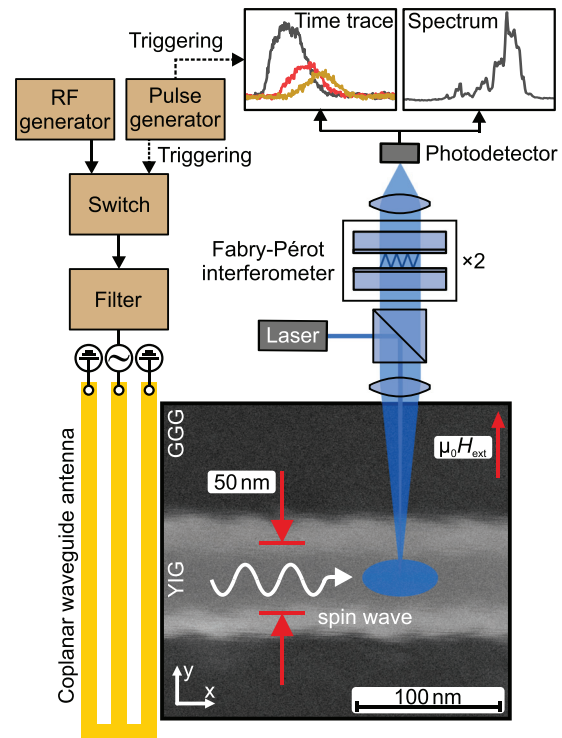


**FIG. 1.** Experimental setup and scanning electron microscopy micrograph of the structure under investigation. A large bias magnetic field of  $\mu_0 H_{\text{ext}} = 270$  mT is used to magnetize the waveguide along the short axis ( $y$ -direction). Spin-wave packets are generated by feeding RF current pulses into a CPW antenna on top of the YIG waveguide. Frequency and spatial and time-resolved scans are performed using microfocused BLS. The structure exhibits a trapezoidal cross section with top and bottom widths of 50 nm and 85 nm, respectively, caused by the fabrication process. The spin-wave wavelength and laser spot size are not up to the scale.

using an RF generator in combination with a fast switch and filter elements. Subsequently, propagating spin-wave packets are excited in the YIG waveguide and are detected using microfocused BLS spectroscopy. A single-frequency laser operating at 457 nm is used, which is focused through the substrate of the sample on the structure using a compensating microscope objective (magnification 100 $\times$  and numerical aperture NA = 0.85). In-plane spin-wave wavevectors up to  $k = 24$  rad  $\mu\text{m}^{-1}$  can be detected. The laser spot diameter is approximately 300 nm, and the effective laser power on the sample is 5 mW. To support the findings, micromagnetic simulations are performed using the MuMax3 open source framework.<sup>34</sup> The trapezoidal waveguide is modeled with the following dimensions: 20  $\mu\text{m}$  length, 85 nm and 50 nm bottom and top width, respectively, and 44 nm thickness. The cell size is  $10 \times 2.5 \times 5.5$  nm<sup>-3</sup>, thus introducing eight thickness layers with varying discrete widths. The material parameters of the plain film are used in the simulations since it has been shown that the structuring process only has a moderate influence on the structure properties.<sup>15</sup> An external magnetic field of  $\mu_0 H_{\text{ext}} = 270$  mT is applied in-plane along the short axis of the structure, and a ground state is prepared by relaxing a random magnetization distribution. Afterward, a driving magnetic field is applied with a spatial field distribution corresponding to the CPW antennas magnetic field to excite spin-

wave packets. Time- and spatial Fourier transformations allow to extract the dispersion relationship and connected parameters.

First, the spin-wave spectra are investigated for the case of a cw microwave excitation. The results are presented in Fig. 2 for different distances to the CPW antenna,  $1.5 \mu\text{m}$  [Fig. 2(a)] and  $7 \mu\text{m}$  [Fig. 2(b)], respectively. The applied microwave power is varied to reveal the possible occurrence of nonlinear scattering processes, which would act as additional loss channels and influence a measurement of the decay length of the system. As shown in Fig. 2(a), the shape of the spectrum is conserved for different applied powers, thus indicating that no strong nonlinear effects arise in the selected microwave power range. The observed spectrum has a spectral width of 300 MHz and shows a complex behavior, which might be attributed to microwave transmission characteristics of the used CPW antenna. Comparison of the spectral distribution close to the antenna with the distribution after several micrometers of propagation [Fig. 2(b)] reveals that the low-frequency part of the spectrum is strongly attenuated. These states are likely close to the ferromagnetic resonance of the structure and, thus, as it is shown in the following, exhibit only a small group velocity.

To support the findings, micromagnetic simulations are conducted using a sinc-function pulse to realize a broadband excitation of the whole dispersion relation. In Fig. 3(a), the resulting excited spectrum is shown for the experimentally accessible wavevector range. A clear single-mode state in frequency is observed following a monotonous function. However, the absolute frequency is shifted by approximately 300 MHz with respect to the experimental results of Fig. 2, which indicates that the magnetic parameters are slightly alternated by the structuring process.<sup>13</sup> In addition, a small variation of the magnetic width of the structure can also significantly impact the spin-wave frequency on the present scale. The various small gaps in the dispersion relationship are caused by the wavevector selective excitation efficiency of the CPW antenna, as shown in Fig. 3(b). Here, the efficiency is approximated by the spatial Fourier transformation of the in-plane field distribution; for a detailed discussion, see Ref. 35. The simulated internal field distribution of the ground state is shown in Fig. 3(c). As expected, large demagnetizing fields arise leading to a strongly

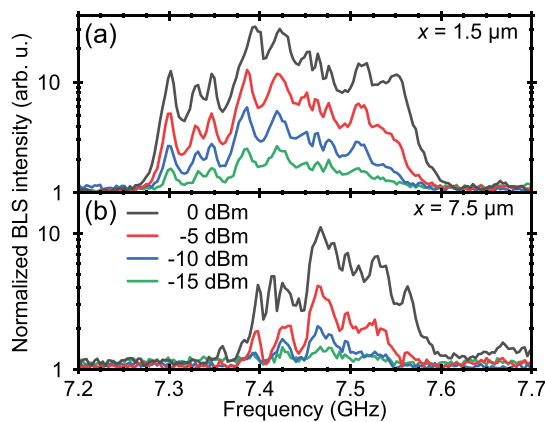


**FIG. 2.** Spin-wave spectra dependent on the applied microwave power. Continuous-excitation spin-wave spectra are measured at distances of (a)  $1.5 \mu\text{m}$  and (b)  $7 \mu\text{m}$  from the CPW antenna. Low frequency states close to the ferromagnetic resonance are strongly attenuated. The spectra are normalized with respect to the thermal noise level.

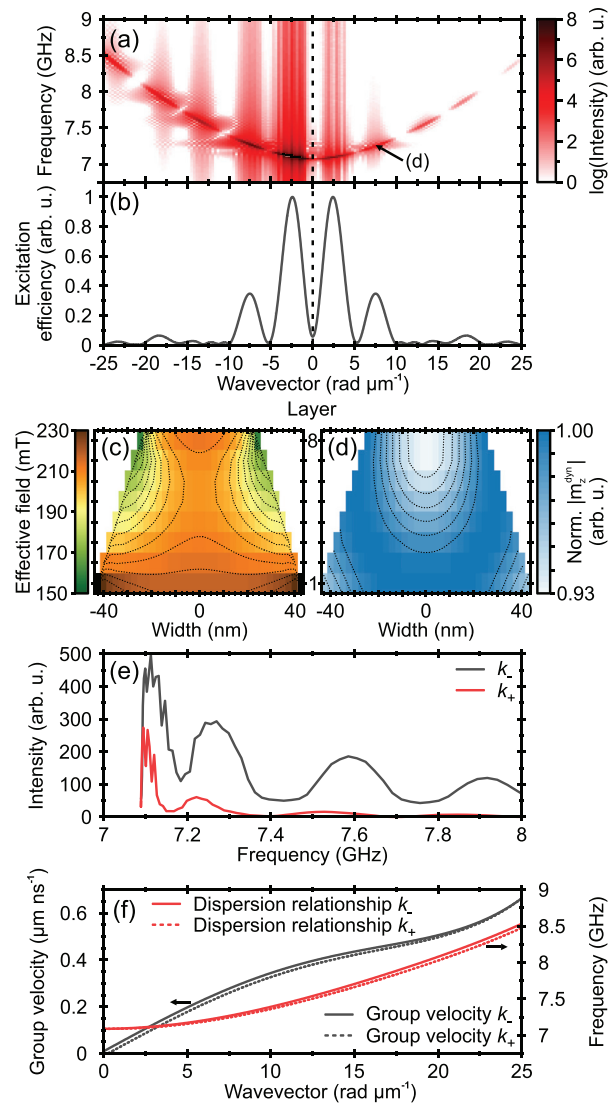


**FIG. 3.** Micromagnetic simulations of the investigated structure. (a) The dispersion relationship shows a distinct single-mode behavior in the experimentally accessible wavevector range. Logarithm of the intensity is displayed. (b) Excitation efficiency of the CPW antenna, approximated by the spatial Fourier transformation of the in-plane field distribution. The wavevector selectivity causes several gaps, visible in (a). (c) Y-component of the internal magnetic field of the ground state. The distribution of the internal magnetic field along the y-direction is strongly inhomogeneous. (d) Normalized absolute value of the dynamic out-of-plane magnetization component  $|m_z^{(d)}|$  for a frequency of 7.26 GHz and  $k = 7.5 \text{ rad } \mu\text{m}^{-1}$ . The profile is rather homogeneous (note the scale from 0.93 to 1). (e) The extracted spectral distribution shows a large intensity difference for counter-propagating spin waves. Comparison of the spectral width with Fig. 2 indicates that the experiment is limited to the first two excitation efficiency maxima of the CPW antenna. (f) A small frequency nonreciprocity for counter-propagating waves is found in the dispersion relation, which is caused by the trapezoidal cross section of the structure. The group velocity is much larger than that for waves of the corresponding longitudinal magnetized state.

nonuniform internal field distribution along the external magnetic field direction. Similar to micrometer-sized conduits, distinct regions of a significantly reduced effective magnetic field are formed at the edges of the structure. However, in contrast to the typically observed



edge mode and center mode states,<sup>28–30</sup> the mode is neither localized in the center nor at the edges of the structure, as it can be seen from the mode profile (normalized absolute value of the dynamic out-of-plane magnetization component  $|m_z^{\text{dyn}}|$ ), shown in Fig. 3(d) for a frequency of 7.26 GHz and  $k = 7.5 \text{ rad } \mu\text{m}^{-1}$ . The profile is rather homogeneous across the width and extends fully into the edge regime of the structure. Additional simulations for different structure widths (see the supplementary material) reveal that the investigated mode is actually the formerly localized edge mode observed in larger structures, which continuously transforms into a homogeneous mode for decreasing width. In contrast, the former mode localized in the center is strongly lifted in frequency due to the increasing quantization and the associated strong exchange contribution. Thus, a broad single-mode frequency range is established and a true edge mode is not present in the system.

Extraction of the respective spectral distribution, see Fig. 3(e), shows an intensity difference for counter-propagating waves ( $k_-$  and  $k_+$ ), which is caused by a nonreciprocal excitation efficiency of the MSSW when using a microwave antenna.<sup>8,35</sup> Moreover, comparison of the spectra with Fig. 2 indicates that the experiment is limited to the first two excitation efficiency maxima of the CPW antenna. Excitation maxima of higher order are likely not observed due to the limited sensitivity of the used BLS setup, especially due to the small amount of probed material and the background of thermal spin waves, leading to an increased noise level in the experiment.

In Fig. 3(f), the dispersion relationship, derived from a sixth-order polynomial approximation of Fig. 3(a), and the group velocity, extracted as the derivative of the dispersion relationship, are shown. Similar to microscopic systems (see the supplementary material), the transversely magnetized state offers a high and much larger group velocity than the waves of the corresponding longitudinal magnetized state.<sup>13</sup>

In the following, the group velocity and the decay length are determined experimentally by a direct measurement of propagating spin-wave packets to further characterize the system and investigate whether a long range spin-wave propagation can be realized in such nano-scaled systems. Thus, a pulsed excitation with a pulse length of 50 ns and a repetition time of 350 ns is used, choosing an applied microwave power of  $-10 \text{ dBm}$  to ensure an operation within the linear regime. In Fig. 4(a), time-resolved BLS measurements of the excited spin-wave packets are shown for different positions along the conduit. The respective center-of-mass arrival time of the pulse is determined by subtracting the thermal noise and calculating the weighted average of the packet. A linear approximation of the packet arrival time, as shown in Fig. 4(b), yields the group velocity  $v_g$ . Additionally, the decay length can be extracted from the integrated pulse intensity of each position by approximating the decay as follows:

$$I = I_1 \exp(-2x/\lambda_D) + I_0. \quad (1)$$

Here,  $I_1$  denotes the initial intensity,  $I_0$  the offset intensity,  $x$  the position, and  $\lambda_D$  the decay length. Extracted according to this principle, the resulting group velocities and decay lengths are presented in Fig. 4(c). The velocity lies within the expected range predicted by the simulations when compared for wavevectors up to  $10 \text{ rad } \mu\text{m}^{-1}$ , see Fig. 3(f), and follows the rising trend to higher frequencies. However, an unexpected large velocity is observed for the smallest investigated frequency not covered by the prediction of the simulations. This might

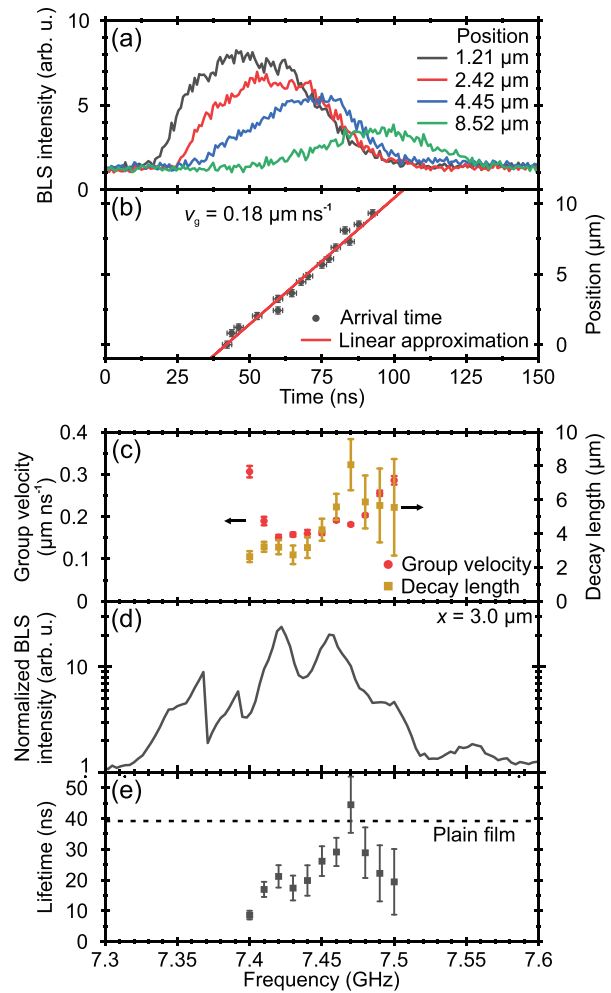


**FIG. 4.** (a) Spin-wave pulses detected at different distances from the CPW antenna for a chosen excitation frequency of 7.47 GHz. (b) Center-of-mass arrival time of the spin-wave pulses of (a). A linear approximation yields the group velocity of the wave packets. (c) Group velocity for various excitation frequencies extracted according to the principle presented in (a) and (b). The decay length is calculated from the integrated intensity of the spin-wave pulses. The associated cw excitation spectrum shown in (d) is slightly shifted to lower frequencies due to a magnetic field difference of 0.2 mT compared to (c). (e) Experimental lifetime derived from the decay length and group velocity. All data are measured for an applied power of  $-10 \text{ dBm}$ .

be an artifact attributed to an additional influence of the out-of-plane excitation field components, which are not localized at the antenna but reach a certain distance along the waveguide. This excitation has the largest efficiency for small wavevectors (frequencies closer to  $k = 0$ ) and drops off significantly for larger wavevectors. In contrast, the decay length follows a steep increase up to a maximum of  $(8.0 \pm 1.5) \mu\text{m}$ , slightly dropping off for higher frequencies. For comparison, the corresponding cw excitation spectrum is displayed in Fig. 4(d), which is, however, slightly shifted to smaller frequencies due to a small magnetic field difference of 0.2 mT. Taking this shift into account, the second spectral peak matches the frequency of the

maximum decay length. We would like to point out that the observed decay length of  $8.0 \mu\text{m}$  is significantly larger in comparison to reported values in the longitudinal magnetization configuration of  $1.8 \mu\text{m}$ .<sup>13</sup> This potentially enables complex nano-sized integrated spin-wave circuits consisting of multiple elements without any means of intermediate amplification, severely lowering the energy consumption of such circuits.

In the following, the lifetime  $\tau$  of the propagating waves, shown in Fig. 4(e), is derived from the experimental results using the following expression:<sup>22</sup>

$$\tau = \lambda_D/v_g. \quad (2)$$

Here, a rather large lifetime of up to  $(44.7 \pm 9.1)$  ns is found. Calculating the lifetime of the ferromagnetic resonance of the plain film as a comparison,<sup>22</sup> considering the decreased internal magnetic field of the transverse magnetization state, results in 112.5 ns for only Gilbert type losses and 39.2 ns taking the full linewidth into account. Here, two effects likely take place affecting the considerations: on the one hand, the structuring procedure influences the material parameters<sup>13</sup> and potentially reduces the lifetime compared to the plain film. On the other hand, the nonlocal inhomogeneous linewidth broadening extracted from the plain film overestimates the effective inhomogeneity on the length scale of the nano-structure.<sup>36</sup> Thus, a comparison to the full linewidth of the plain film can yield a lifetime smaller than the lifetime of the nano-structure. Nonetheless, the measured lifetime exceeds other commonly used materials such as Permalloy<sup>37</sup> by far, even when compared to microscopic or macroscopic systems.

Finally, we would like to discuss a peculiarity of the investigated system, observed in Fig. 3(f). The simulated dispersion relationship exhibits a small frequency nonreciprocity, which is caused by the trapezoidal cross section of the structure and the associated internal field distribution [Fig. 3(c)]. This introduces an additional spatial symmetry break, similar to the case of magnetic bilayers.<sup>38</sup> In Fig. 5, two measured spectra for normal and inverted field polarity are shown, which equal a switch of the dispersion branch from  $k_{-/+}$  to  $k_{+/-}$ . Indeed, a

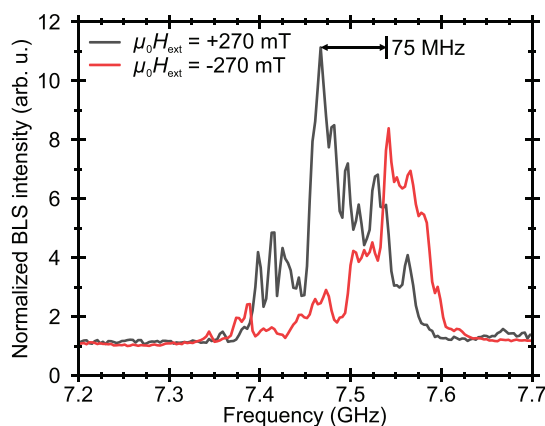


**FIG. 5.** Frequency nonreciprocity of counter-propagating spin waves. Inverting the field polarity equals the switching of the propagation direction for the spin waves. A frequency shift of 75 MHz is observed. The spectra are recorded for an applied power of 0 dBm at a distance of  $7 \mu\text{m}$  from the CPW antenna. Normalization is performed with respect to the thermal noise level.

distinct nonreciprocity with a frequency shift of 75 MHz is found, which is substantially larger than the predicted shift of 20 MHz–30 MHz for spin waves in the range of  $7 \text{ rad } \mu\text{m}^{-1}$ – $10 \text{ rad } \mu\text{m}^{-1}$  [see Fig. 3(f)]. It should be noted that the observed frequency shift is likely influenced by the nonreciprocal excitation efficiency for both configurations, leading to different spin-wave densities and, thus, to a different nonlinear frequency downshift potentially increasing the observed frequency gap. In the [supplementary material](#), the absence of the nonreciprocity for a rectangular cross section is shown and additional influences are discussed. Nonetheless, such a pronounced nonreciprocity is of particular interest for an application in spin-wave devices since it allows for, e.g., the construction of a nano-sized spin-wave diode.

To conclude, we presented a study of propagating spin-wave packets in a transversely magnetized nano-scaled YIG conduit of 50 nm width. Micromagnetic simulations are performed to support the experimental findings, revealing a broad single-mode frequency range. It is shown that the investigated mode originates from an edge mode but, in contrast to the common localized edge modes in microscopic systems, has a rather homogeneous distribution across the width of the structure. A large spin-wave group velocity is measured and a long-range spin-wave propagation is observed with a decay length of up to  $(8.0 \pm 1.5) \mu\text{m}$ , which is multiple times larger than reported values for the corresponding longitudinal magnetized state.<sup>13</sup> In addition, a large spin-wave lifetime of up to  $(44.7 \pm 9.1)$  ns is found. Furthermore, a frequency nonreciprocity for counter-propagating spin waves is observed and experimentally verified, which is caused by the trapezoidal cross section of the structure and the associated internal field distribution. This nonreciprocity and the revealed long-distance spin-wave propagation on the nano-scale are particularly interesting for an application in spin-wave devices, allowing for long-distance transport of information in magnonic circuits and low-energy device architectures potentially opening up the path to multi-element circuits without intermediate amplification.

See the [supplementary material](#) for additional information on the origin of the investigated mode and the mode spectrum for different waveguide widths and a discussion of the group velocity for transverse and longitudinal magnetized microscopic waveguides.

This research was funded by the European Research Council project ERC Starting Grant No. 678309 MagnonCircuits, by the Deutsche Forschungsgemeinschaft (DFG, German Research Foundation)–No. 271741898—by Collaborative Research Center No. SFB/TRR 173-268565370 (Project B01), and by the Austrian Science Fund (FWF) through Project No. I 4696-N. B.H. acknowledges support from the Graduate School Material Science in Mainz (MAINZ). The authors thank Burkard Hillebrands for support and valuable discussions.

#### DATA AVAILABILITY

The data that support the findings of this study are available from the corresponding author upon reasonable request.

#### REFERENCES

- 1A. Khitun, M. Bao, and K. L. Wang, *J. Phys. D* **43**, 264005 (2010).

- <sup>2</sup>V. V. Kruglyak, S. O. Demokritov, and D. Grundler, *J. Phys. D* **43**, 260301 (2010).
- <sup>3</sup>A. V. Chumak, V. I. Vasyuchka, A. A. Serga, and B. Hillebrands, *Nat. Phys.* **11**, 453 (2015).
- <sup>4</sup>A. Mahmoud, F. Ciubotaru, F. Vanderveken, A. V. Chumak, S. Hamdioui, C. Adelman, and S. Cotofana, *J. Appl. Phys.* **128**, 161101 (2020).
- <sup>5</sup>Y. Kajiwara, K. Harii, S. Takahashi, J. Ohe, K. Uchida, M. Mizuguchi, H. Umezawa, H. Kawai, K. Ando, K. Takanashi, S. Maekawa, and E. Saitoh, *Nature* **464**, 262 (2010).
- <sup>6</sup>H. Yu, O. D. Kelly, V. Cros, R. Bernard, P. Bortolotti, A. Anane, F. Brandl, R. Huber, I. Stasinopoulos, and D. Grundler, *Sci. Rep.* **4**, 6848 (2014).
- <sup>7</sup>C. Dubs, O. Surzhenko, R. Thomas, J. Osten, T. Schneider, K. Lenz, J. Grenzer, R. Hübner, and E. Wandler, *Phys. Rev. Mater.* **4**, 024416 (2020).
- <sup>8</sup>T. Schneider, A. A. Serga, B. Leven, B. Hillebrands, R. L. Stamps, and M. P. Kostylev, *Appl. Phys. Lett.* **92**, 022505 (2008).
- <sup>9</sup>P. Krivosik and C. E. Patton, *Phys. Rev. B* **82**, 184428 (2010).
- <sup>10</sup>V. E. Demidov, J. Jersch, K. Rott, P. Krzysteczko, G. Reiss, and S. O. Demokritov, *Phys. Rev. Lett.* **102**, 177207 (2009).
- <sup>11</sup>A. V. Sadovnikov, E. N. Beginin, M. A. Morozova, Y. P. Sharaevskii, S. V. Grishin, S. E. Sheshukova, and S. A. Nikitov, *Appl. Phys. Lett.* **109**, 042407 (2016).
- <sup>12</sup>Q. Wang, B. Heinz, R. Verba, M. Kewenig, P. Pirro, M. Schneider, T. Meyer, B. Lägel, C. Dubs, T. Brächer, and A. V. Chumak, *Phys. Rev. Lett.* **122**, 247202 (2019).
- <sup>13</sup>B. Heinz, T. Brächer, M. Schneider, Q. Wang, B. Lägel, A. M. Friedel, D. Breitbach, S. Steinert, T. Meyer, M. Kewenig, C. Dubs, P. Pirro, and A. V. Chumak, *Nano Lett.* **20**, 4220 (2020).
- <sup>14</sup>T. Brächer and P. Pirro, *J. Appl. Phys.* **124**, 152119 (2018).
- <sup>15</sup>Á. Papp, W. Porod, Á. I. Csurgay, and G. Csaba, *Sci. Rep.* **7**, 9245 (2017).
- <sup>16</sup>Q. Wang, M. Kewenig, M. Schneider, R. Verba, F. Kohl, B. Heinz, M. Geilen, M. Mohseni, B. Lägel, F. Ciubotaru, C. Adelman, C. Dubs, S. D. Cotofana, O. V. Dobrovolskiy, T. Brächer, P. Pirro, and A. V. Chumak, *Nat. Electron.* **3**, 765–774 (2020).
- <sup>17</sup>T. Fischer, M. Kewenig, D. A. Bozhko, A. A. Serga, I. I. Svyrotka, F. Ciubotaru, C. Adelman, B. Hillebrands, and A. V. Chumak, *Appl. Phys. Lett.* **110**, 152401 (2017).
- <sup>18</sup>G. Talmelli, T. Devolder, N. Träger, J. Förster, S. Wintz, M. Weigand, H. Stoll, M. Heyns, G. Schütz, I. P. Radu, J. Gräfe, F. Ciubotaru, and C. Adelman, *Sci. Adv.* **6**, eabb4042 (2020).
- <sup>19</sup>Q. Wang, A. Hamadeh, R. Verba, V. Lomakin, M. Mohseni, B. Hillebrands, A. V. Chumak, and P. Pirro, *npj Comput. Mater.* **6**, 192 (2020).
- <sup>20</sup>Á. Papp, W. Porod, and G. Csaba, “Nanoscale neural network using non-linear spin-wave interference,” *arXiv:2012.04594* (2020).
- <sup>21</sup>Q. Wang, A. V. Chumak, and P. Pirro, “Inverse-design magnonic devices,” *arXiv:2012.04544* (2020).
- <sup>22</sup>A. G. Gurevich and G. A. Melkov, *Magnetization Oscillations and Waves* (CRC Press, 1996).
- <sup>23</sup>E. Iacocca and O. Heinonen, *Phys. Rev. Appl.* **8**, 034015 (2017).
- <sup>24</sup>X. S. Wang, H. W. Zhang, and X. R. Wang, *Phys. Rev. Appl.* **9**, 024029 (2018).
- <sup>25</sup>K. Yamamoto, G. C. Thiang, P. Pirro, K.-W. Kim, K. Everschor-Sitte, and E. Saitoh, *Phys. Rev. Lett.* **122**, 217201 (2019).
- <sup>26</sup>M. Mohseni, B. Hillebrands, P. Pirro, and M. Kostylev, *Phys. Rev. B* **102**, 014445 (2020).
- <sup>27</sup>U. K. Bhaskar, G. Talmelli, F. Ciubotaru, C. Adelman, and T. Devolder, *J. Appl. Phys.* **127**, 033902 (2020).
- <sup>28</sup>C. Bayer, J. P. Park, H. Wang, M. Yan, C. E. Campbell, and P. A. Crowell, *Phys. Rev. B* **69**, 134401 (2004).
- <sup>29</sup>G. Gubbiotti, M. Conti, G. Carlotti, P. Candeloro, E. D. Fabrizio, K. Y. Guslienko, A. Andre, C. Bayer, and A. N. Slavin, *J. Phys.* **16**, 7709 (2004).
- <sup>30</sup>P. Pirro, T. Brächer, A. V. Chumak, B. Lägel, C. Dubs, O. Surzhenko, P. Görnert, B. Leven, and B. Hillebrands, *Appl. Phys. Lett.* **104**, 012402 (2014).
- <sup>31</sup>C. Dubs, O. Surzhenko, R. Linke, A. Danilewsky, U. Bräckner, and J. Dellith, *J. Phys. D* **50**, 204005 (2017).
- <sup>32</sup>I. S. Maksymov and M. Kostylev, *Physica E* **69**, 253 (2015).
- <sup>33</sup>T. Sebastian, K. Schultheiss, B. Oby, B. Hillebrands, and H. Schultheiss, *Front. Phys.* **3**, 35 (2015).
- <sup>34</sup>A. Vansteenkiste, J. Leliaert, M. Dvornik, M. Helsen, F. Garcia-Sanchez, and B. Van Waeyenberge, *AIP Adv.* **4**, 107133 (2014).
- <sup>35</sup>V. E. Demidov, M. P. Kostylev, K. Rott, P. Krzysteczko, G. Reiss, and S. O. Demokritov, *Appl. Phys. Lett.* **95**, 112509 (2009).
- <sup>36</sup>C. Hahn, V. V. Naletov, G. de Loubens, O. Klein, O. d’Allivy Kelly, A. Anane, R. Bernard, E. Jacquet, P. Bortolotti, V. Cros, J. L. Prieto, and M. Muñoz, *Appl. Phys. Lett.* **104**, 152410 (2014).
- <sup>37</sup>K. Yamanoi, S. Yakata, T. Kimura, and T. Manago, *Jpn. J. Appl. Phys., Part 1* **52**, 083001 (2013).
- <sup>38</sup>S. Shichi, N. Kanazawa, K. Matsuda, S. Okajima, T. Hasegawa, T. Okada, T. Goto, H. Takagi, and M. Inoue, *J. Appl. Phys.* **117**, 17D125 (2015).